VERSITA

OPTO-ELECTRONICS REVIEW **22**(3), 147–151

DOI: 10.2478/s11772-014-0194-y

ATLAS simulation of a laser diode for free space optical communication (FSOC) in mid-infrared spectral region

SANJEEV[1] and P. CHAKRABARTI[2*]

[1]Department of Electronics and Instrumentation Engineering, Faculty of Engineering and Technology, MJP Rohilkhand University, Bareilly – 243 006 India
[2]Centre for Research in Microelectronics (CRME), Department of Electronics Engineering, Indian Institute of Technology (BHU), Varanasi – 221 005 India

In this paper, simulation studies on an N^+-$InAs_{0.61}Sb_{0.13}P_{0.26}$/$n^0$-$InAs_{0.97}Sb_{0.03}$/$P^+$-$InAs_{0.61}Sb_{0.13}P_{0.26}$ double heterostructure laser diode suitable for use as a source in a free space optical communication system at 3.7 μm at room temperature has been presented. The device structure has been characterized in terms of energy band diagram, electric field profile, and carrier concentration profile using ATLAS simulation tool from Silvaco. The current-voltage characteristics of the structure have been estimated taking into account the degeneracy effect. The results of simulation have been validated by the reported experimental results.

Keywords: ATLAS, free space optical communication, laser diode, mid-infrared, simulation.

1. Introduction

The 3–5 μm spectral region is becoming of interest for the free space optical communication (FSOC) because of the availability of low loss atmospheric windows in this range [1]. The advantages of the free space optical communication includes high bandwidth, eye safe, license free operation, high transmission security, protocol transparency, jam--proof and error free link. The sources for a free space optical communication system require a narrow bandgap semiconductor materials for their fabrication. The $InAs_{1-x}Sb_x$/$InAs_{1-x-y}Sb_xP_y$ semiconductor alloys are promising materials for the design and fabrication of high power mid-infrared lasers with the emission wavelength in the range from 3 μm to 5 μm. The continuous room temperature operation of these sources is limited by non-radiative recombination such as Shockley-Read-Hall (SRH) and Auger recombination, which are the dominating recombination mechanisms in narrow bandgap semiconductors, especially at high injection, which prevails in the laser operation. Several experimental laser structures have been reported for operation in a 3–5 μm spectral range recently [2–5] for a number of mid-infrared applications including a free space optical communication. However, rigorous theoretical studies received comparatively less attention. Analytical studies based on a closed form simulation are of little help in understanding various complex mechanisms that shape the characteristics of the device under actual operating conditions. This is because; closed form models are based on drastic assumptions which are not valid for a practical device. On the other hand, it is possible to use advanced software simulation tools to model such complex devices by incorporating user defined model equations as required in a particular case. At present it is necessary to address the various issues theoretically to characterize injection laser sources for room temperature continuous operation in the mid-infrared spectral region for free space optical communication. The present paper makes use of the ATLAS simulation platform to model an $InAs_{1-x}Sb_x$/$InAs_{1-x-y}Sb_xPy$ laser for the proposed application.

2. The device structure

The device under consideration is based on an N^+-$InAs_{0.61}Sb_{0.13}P_{0.26}$/$n^0$-$InAs_{0.97}Sb_{0.03}$/$P^+$-$InAs_{0.61}Sb_{0.13}P_{0.26}$ semiconductor material system similar to one reported by Yin *et al.* [4]. The schematic of the structure is shown in Fig. 1(a). The ATLAS [6] simulated structure is shown in Fig. 2. The structure consists of two confining layers of thickness t_1 and t_2, respectively of larger bandgap degenerate quaternary materials $InAs_{0.61}Sb_{0.13}P_{0.26}$ of different conductivities and an active layer of thickness d of $InAs_{0.97}Sb_{0.03}$ sandwiched between them to form the double heterostructure. The whole structure is supposed to be grown on the lattice matched p-InAs substrate. The energy band diagram of the proposed DH laser structure has been obtained by applying the classical Anderson Model [7] and is shown in Fig. 1(b). E_{fn} and E_{fp} are the quasi-Fermi level for electrons and holes in the structure. E_{g1} and E_{g2} are the energy bandgap of the confining layer (InAsSbP) and active layer (InAsSb), respec-

*e-mail: pchakrabarti.ece@iitbhu.ac.in

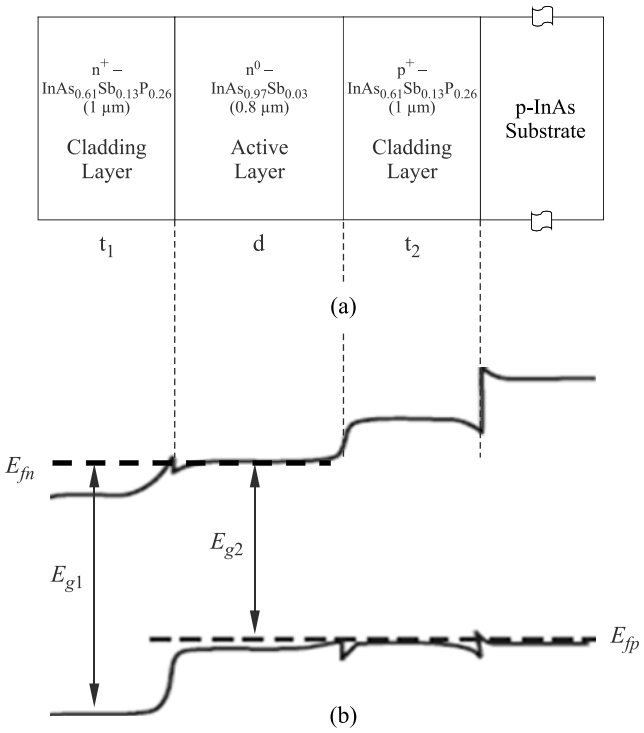

Fig. 1. (a) Schematic of proposed mid-infrared DH laser (b) Energy band diagram.

tively. The proposed ideal DH laser structure forms a Type-I band alignment. The DH laser structure is designed in a way so as to emit near 3.7 μm at 300 K coinciding with the one of the low loss atmospheric windows suitable for a free space optical communication.

The compositional and temperature dependent energy bandgap (E_{g2}) of $InAs_{1-x}Sb_x$ has been calculated using [8]

$$E_{g2}(x,T) = 0.411 - \frac{3.4\times10^{-4}T^2}{210+T} - 0.876x + 0.70x^2 + 3.4\times10^{-4}xT(1-x), \quad (1)$$

where x is the mole-fraction (= 0.03 in our model) and T is the temperature in Kelvin.

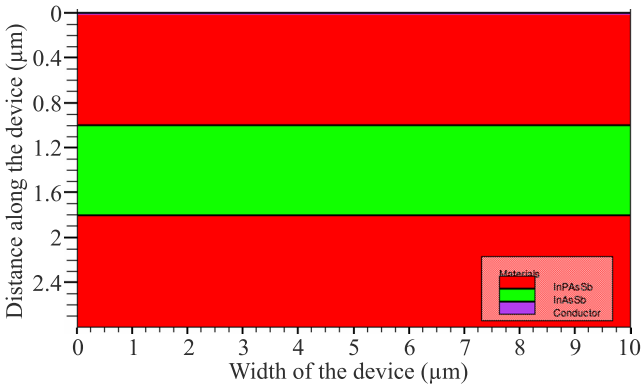

Fig. 2. The proposed structure as simulated by ATLAS.

On the other hand, to the first approximation, the composition dependence of the energy bandgap (E_{g1}) of $InAs_xSb_yP_{1-x-y}$ at room temperature can be expressed as [9]

$$E_{g1} = xE_g(InAs) + yE_g(InSb) + (1-x-y)E_g(InP) - y(1-x-y)C_2 - x(1-x-y)C_1 - xyC_3, \quad (2)$$

where C_1, C_2 and C_3 are the appropriate bowing parameters for InAs, InSb and InP and $E_g(InAs)$, $E_g(InSb)$ and $E_g(InP)$ are the energy bandgap values of InAs, InSb and InP binary semiconductors, respectively at room temperature and are listed in Table 1. The other parameters of quaternary materials (InAsSbP) used in the simulation model have been computed from the parameters of the constituent binary/ternary materials using the linear interpolation technique and some have been incorporated into the simulation codes of ATLAS.

Table 1. Values of parameters used in the model at 300 K [4,10].

Parameter	Value
N_a	1×10^{18} cm^{-3}
N_d	5×10^{18} cm^{-3}
d	0.8 μm
t_1	1.0 μm
t_2	1.0 μm
E_{g1}	0.498 eV (estimated)
E_{g2}	0.328 eV (estimated)
χ_1	4.759 eV (estimated)
χ_2	4.890 eV
m_n^* ($InAs_{1-x}Sb_x$)	$(0.023 - 0.039x + 0.03x^2)m_0$
m_p^* ($InAs_{1-x}Sb_x$)	$(0.026 - 0.011x)m_0$
m_s ($InAs_{1-x}Sb_x$)	$(0.16 - 0.04x)m_0$
m_{hh} ($InAs_{1-x}Sb_x$)	$(0.41 + 0.02x)m_0$
Δ ($InAs_{1-x}Sb_x$)	$(0.39 - 0.75x + 1.17x^2)$ eV
C_1	0.101
C_2	0.20
C_3	0.62
E_g(InAs)	0.35 eV
E_g(InSb)	0.18 eV
E_g(InP)	0.62 eV
Cavity length	500 μm
RF, *RR*	90%

3. The ATLAS simulation model

The structure has been simulated in the Deck-build platform of ATLAS by defining mesh, region, electrode and doping parameters as listed in Table 1 along with other parameters. In the material statement, several material parameters like bandgap, permittivity, density of state of conduction and valance band, mobility and carrier lifetimes value have been provided as per our structure and estimation.

The current-voltage characteristics of the structure have been determined with the help of ATLAS simulation tool by solving the governing charge equation using initial solution statement in the Deck-build coding by considering the

FERMIDIRAC statistics applicable for highly doped degenerate semiconductors. The doping profile, electric field profile, electron-hole concentration under equilibrium and current-voltage characteristics have been plotted using the TONYPLOT tool of ATLAS.

The LASER module of the ATLAS solves the electrical and optical equation self consistently. It solves the Helmholt's equation to calculate the optical field and photon density for the given structure as

$$\nabla_{xy}^2 E_k(x,y)+\left[\frac{\omega_m^2}{c^2}\varepsilon(x,y)-\beta_k^2\right]E_k(x,y)=0, \qquad (3)$$

where ∇_{xy}^2 is the two dimensional Laplace operator, ω_m is the frequency corresponding to longitudinal mode m, c is the velocity of light in vacuum, β_k is the complex Eigen values for corresponding Eigen functions $E_k(x,y)$, and $\varepsilon(x,y)$ is the high frequency dielectric permittivity. The ATLAS takes into account the fundamental transverse mode solution and longitudinal mode with the greatest power and subsequently assumes that

$$E_m(x,y)=E_0(x,y), \qquad (4)$$

where $E_0(x,y)$ is the optical field corresponding to the most powerful longitudinal mode.

The dielectric permittivity has been defined in LASER simulation as

$$\varepsilon(r,z)=\varepsilon_0+(-ALPHAR+j)\frac{\sqrt{\varepsilon_0 g(r,z)}}{k_w} - j\frac{\sqrt{\varepsilon_0}(ALPHAA+FCN\cdot n+FCP\cdot n)}{k_w}, \qquad (5)$$

here *ALPHAR* is the line width broadening factor, *ALPHAA* is the bulk absorption loss, *FCN* and *FCP* are the coefficients of free carrier losses, and $g(r,z)$ is the local optical gain whose value can be modelled as

$$g(r,z)=GAIN0\sqrt{\frac{\hbar\omega-E_g}{kT}}\left\{f\left[\frac{E_c-E_{fn}+GAMMA(\hbar\omega-E_g)}{kT}\right] -f\left[\frac{E_v-E_{fp}-(1-GAMMA)(\hbar\omega-E_g)}{kT}\right]\right\}, \qquad (6)$$

where E_{fn} and E_{fp} are the quasi-Fermi energies for electron and hole, f is defined as

$$f(x)=1/[1+\exp(x)],\quad GAMMA=\frac{1}{(N_c/N_v)^{2/3}+1}$$

and *GAIN*0 can be defined in the MATERIAL statement.

In the carrier generation-recombination models, we have taken the SRH recombination, Radiative recombination, AUGER recombination and stimulated emission models.

The optical generation/recombination rate has been expressed as

$$R_{np}^{OPT}=C_c^{OPT}(np-n_{ie}^2), \qquad (7)$$

where C_c^{OPT} is the capture rate. n, p and n_{ie} are the electron, holes and intrinsic carrier concentration, respectively.

The SRH recombination in ATLAS simulation has been modelled as [6]

$$R_{SRH}=\frac{pn-n_{ie}^2}{TAUP0\left[n+n_{ie}\exp\left(\frac{ETRAP}{kT_L}\right)\right]+TAUN0\left[p+n_{ie}\exp\left(\frac{-ETRAP}{kT_L}\right)\right]}, \qquad (8)$$

where *ETRAP* is the difference between the trap energy level and intrinsic Fermi level, T_L is the lattice temperature in Kelvin and TAUN0 and TAUP0 are the electron and hole lifetimes and are the function of carrier capture cross section and thermal velocity.

The Auger recombination has been modelled as [6]

$$R_{Auger}=AUGN(pn^2-nn_{ie}^2)+AUGP(np^2-pn_{ie}^2), \qquad (9)$$

where *AUGN* and *AUGP* are the model parameters defined in the MATERIAL statement in the ATLAS.

The carrier recombination due to stimulated light emission is modelled as

$$R_{st}(x,y)=\sum_m \frac{c}{NEFF}g(x,y)\left|E(x,y)\right|^2 S_m, \qquad (10)$$

where *NEFF* is the group effective refractive index, S_m is the linear photon density whose value has been found out by solving the photon rate equation and is given by

$$\frac{dS_m}{dt}=\left(\frac{c}{NEFF}G_m-\frac{1}{\tau_{ph_m}}-\frac{c\cdot LOSSES}{NEFF}\right)S_m+R_{sp_m}, \qquad (11)$$

where G_m is the modal gain, R_{sp_m} is the spontaneous emission rate and τ_{ph_m} is the model photon lifetime given by

$$\frac{1}{\tau_{ph_m}}=\frac{c}{NEFF}(\alpha_a+\alpha_{fc}+\alpha_{mir}), \qquad (12)$$

where α_a is the bulk absorption loss, α_{fc} is the free carrier loss and α_{mir} is the mirror loss given by

$$\alpha_{mir}=\frac{1}{2\cdot CAVITY\cdot LENGTH}\ln\left(\frac{1}{RF\cdot RR}\right), \qquad (13)$$

where *CAVITY* · *LENGHT* is the length of cavity of the laser structure, *RF* and *RR* are the percentage reflectivity of the front and rear facet, respectively, whose values are taken from [4] and listed in Table 1.

Finally, the optical power of the laser structure can be given by [6]

$$P_{out}=\frac{h\omega S_m c}{2\cdot NEFF}\left[\frac{\ln(1/RF\cdot RR)}{1+\sqrt{RF/RRR(1-RR)/1-RF}}\right]. \qquad (14)$$

4. Results and discussions

The numerical computation using ATLAS device simulation software has been carried out for mid-infrared P^+-$InAs_{0.61}Sb_{0.13}P_{0.26}$/$n^0$-$InAs_{0.97}Sb_{0.03}$/$N^-$-$InAs_{0.61}Sb_{0.13}P_{0.26}$ double heterostructure laser at 300 K. The various material parameters used in the simulation model are summarized in Table 1.

Figure 3 depicts the built-in electric field profile across the laser structure under no bias condition. The electric fields associated with the P^+-n^0 and n^0-n^+ junctions are triangular in nature and centred at the metallurgical junction with the maximum value of 3×10^4 V/cm and 5.6×10^4 V/cm, respectively.

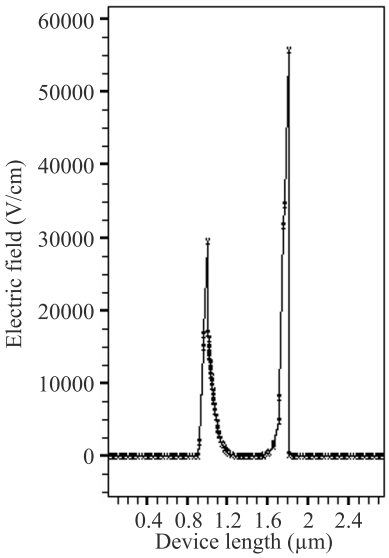

Fig. 3. Electric field profile along the structure.

Figure 4 shows the variation of electron and hole concentration through the structure under unbiased condition. It can be easily verified that variation of hole and electron concentration is complimentary to each other throughout the structure, so as to keep the diffusion current constant throughout the structure. The hole concentration is 10^{18}/cm^3 in the P^+ region and drop to nearly 10^{14}/cm^3 in the active region and becomes 5×10^{18}/cm^3 in the n^+ region. On the other hand the electrons concentration is minimum in the P^+ region with a value of 2×10^9/cm^3 which increases to nearly 10^{16}/cm^3 in the active region. The lightly doped active region ensures that the injection is predominantly from the P^+ region. The electron concentration finally goes up to a value of 5×10^{18}/cm^3 in the n^+ region.

The current-voltage characteristics obtained on the basis of ATLAS simulation are compared and contrasted with the experimentally values reported by others on the same structure at 100 K [4] and is shown in Fig. 5. It can be easily seen that there is a very good agreement between the simulated results and those reported by others. It is further seen that the deviation between the two results increase at higher bias voltage. This is attributed to the fact that at higher bias voltage a larger injection of carriers causes changes of various parameters like minority carrier lifetime, threshold current density due to the change of junction temperature. The temperature dependence of these parameters is not modelled in the present simulation. Figure 6 depicts the variation of the normalized optical output power with bias current density of the laser structure. There is a good agreement between the results obtained on the basis of ATLAS simulation and experimental results reported for the same structure by Yin *et al.* [4]. A larger departure of the simulated results from the experimentally measured values is attributed to the factors mentioned before. It may be further pointed out that in the simulation the effect of interface charges have been completely neglected. This assumption is not true for practical device reported in Ref. 4. The normalization of optical power in Fig. 6 takes care of this factor for the purpose of comparison.

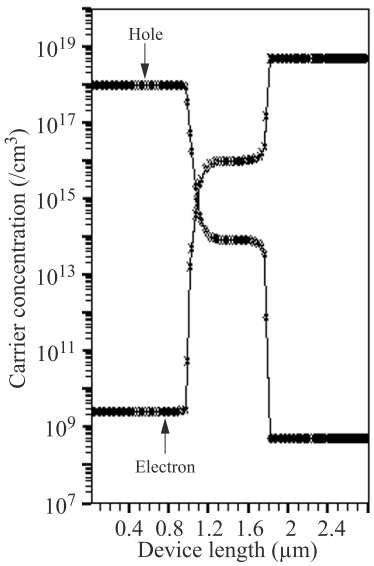

Fig. 4. Variation of carrier concentration in the structure.

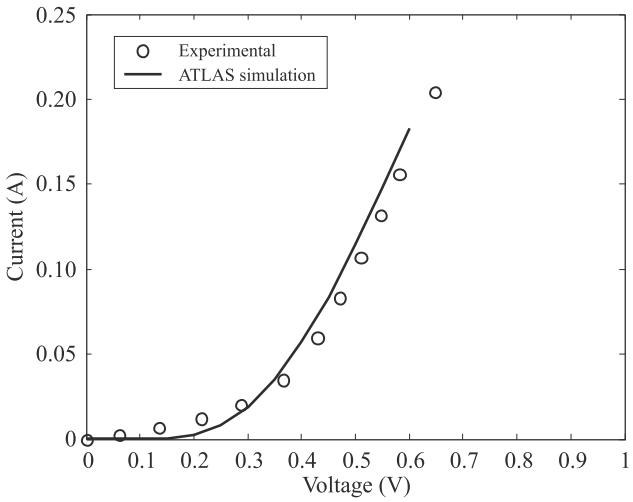

Fig. 5. Current-voltage characteristics of DH-Laser showing the simulated results against the reproduced experimental data reported by others [4].

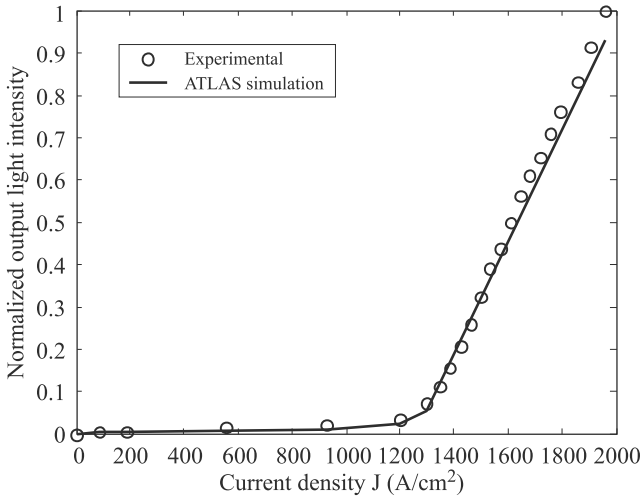

Fig. 6. Output power with the bias current density of the DH-Laser showing simulated results along with experimental data reproduced from the results reported by Yin et al [4].

5. Conclusions

The DH-laser structure have been simulated using ATLAS device simulation package in terms of the energy band diagram, electric field profile, current-voltage characteristics and output power. The degeneracy effect has been considered for calculating the current-voltage characteristics. The results of the ATLAS simulation studies are found to be in good agreement with the experimental results reported by others, which ensures the validity of our model. It is expected that simulation codes developed for the structure, can be used for improving and optimizing the existing structures and development of efficient device prototypes.

Acknowledgement

One of the authors (Sanjeev) would like to acknowledge the financial support from the Council of Science and Technology-UP, Lucknow for this work in the form of a research project.

References

1. S. Narasimha Prasad, "Optical communications in the mid--wave IR spectral band", *J. Opt. Fiber Commun. Rep.* **2**, 558–602 (2005).
2. T.N. Danilova, A.N. Imenkov, V.V. Sherstnev, and Yu.P. Yakovlev, "InAsSb/InAsSbP double heterostructure lasers emitting at 3–4 μm: Part-I", *Semiconductors* **34**, 1343–1350 (2000).
3. T. Ashley, "Type-I InSb-based mid-infrared diode lasers", *Phil. Trans. R. Soc. Lond.* **A359**, 475–488 (2001).
4. M. Yin, A. Krier, S. Krier, R. Jones, and P. Carrington, "Mid-infrared diode lasers for free space optical communications", *Proc. SPIE* **6399**, 63990C1–C6 (2006).
5. A. Krier, M. Yin, V. Smirnov, P. Batty, P.J. Carrington, V. Solovev, and V. Sherstnev, "Development of room temperature LED and lasers for the mid-infrared spectral region", P*hys. Stat. Ssol.* **A 205**, 129–143 (2008).
6. Silvaco Inc., *ATLAS user's manual-A device simulator software*, www.silvaco.com, 2005.
7. B.L. Sharma and R.K. Purohit, *Semiconductor Heterojunctions*, Pergamon Press, Oxford, 1974.
8. A. Rogalski, K. Adamiec, and J. Rutkowski, *Narrow-Gap Semiconductor Photodiode*, SPIE Press, Bellingham, 2000.
9. E.R. Gertner, D.T. Cheung, A.M. Andrews, and J.T. Longo, "Liquid phase epitaxial growth of $InAs_xSb_yP_{1-x-y}$ layers on InAs", *J. Electron. Mater.* **6**, 163–172 (1977).
10. M. Levinshtein, S. Rumyantsev, and M. Shur, *Handbook Series on Semiconductor Parameters, vol.-2*, World Scientific, Singapore, 1996.